Chinese Chemical Letters 32 (2021) 1037–1040

Contents lists available at ScienceDirect

Chinese Chemical Letters

journal homepage: www.elsevier.com/locate/cclet

Communication

Morphology controllable conjugated network polymers based on AIE-active building block for TNP detection

Shan Jiang[a], Lingchen Meng[a], Wenyue Ma[a], Qingkai Qi[a], Wei Zhang[b], Bin Xu[a], Leijing Liu[a,*], Wenjing Tian[a,*]

[a] State Key Laboratory of Supramolecular Structure and Materials, Jilin University, Changchun 130012, China
[b] Electron Microscopy Center, Jilin University, Changchun 130012, China

ARTICLE INFO

Article history:
Received 4 July 2020
Received in revised form 11 September 2020
Accepted 14 September 2020
Available online 15 September 2020

Keywords:
Conjugated network polymers
Aggregation-induced emission
Morphology
2,4,6-Trinitrophenol
Detection

ABSTRACT

Luminescent conjugated network polymer is one of the most promising chemo-sensors owing to their good chemical/optical stability and multiple functionalization. Herein, three conjugated network polymers were prepared by using aggregation-induced emission active 1,1,2,2-tetrakis(4-formyl-(1,1′-biphenyl))-ethane (TFBE) unit as monomer and hydrazine as linker. Through regulating the synthetical condition, the polymeric network can form either uniform two-dimensional azine-linked nanosheets (A-NS), conjugated microporous polymers (A-CMP) or covalent organic frameworks (A-COF). All of these polymers exhibited good stability and high fluorescence quantum efficiency with the quantum yield of 6.31% for A-NS, 5.26% for A-CMP, and 5.80% for A-COF, as well as fast and selective fluorescence quenching response to 2,4,6-trinitrophenol (TNP). And the best TNP sensing performance with the Stern-Volmer constants (K_{sv}) values up to 8×10^5 L/mol and a detection limit of 0.09 μmol/L was obtained for A-NS. The study explores various strategies to construct conjugated polymers with different nanoarchitectures based on the same building block for sensitive detection of explosives.

Conjugated network polymers have attracted more and more attention due to their increasing applications in organic optoelectronic devices [1], photocatalysis and eletrocatalysts [2], sensors [3], energy storage [4], and bioprobes [5]. Luminescent conjugated network polymers is one of the most promising chemo-sensors for volatile chemicals [6], biomolecules [7], metal ions [8], gases [9] and explosives [10] owing to their good chemical/optical stability and multiple functionalization [11]. In most applications, it is necessary for the luminescent covalent organic networks to have high fluorescence quantum efficiency in aggregated states. But conventional polymers often suffer from aggregation-induced quenching (ACQ) effect in their concentrated solution and solid state. While conjugated polymers with aggregation-induced emission (AIE) characteristics can overcome ACQ effect because of the restricted intramolecular motion of the monomer and super amplification effect, resulting in high fluorescence quantum efficiency in solid state [12].

The morphology of luminogenic conjugated network polymers is a key factor that influences their characteristics and even practical applications [13]. Scientists have been making the effort to construct conjugated polymers with controllable morphologies and nanostructures by tuning the building blocks or synthesis conditions. Up to now, a variety of fluorescent conjugated organic polymers with multiple architectures, including nanoparticles [14], micro/nanospheres [15], nanotubes [16], two-dimensional nanosheets [17], conjugated microporous polymers (CMP) [18] and covalent organic frameworks (COF) [19], have been prepared and are widely applied in drug delivery [20], sensing [16], solar cells [21], separation [22], and storage [23] by virtue of their morphological advantages. Thanks to their fascinating high fluorescence quantum efficiency in aggregation state, AIE-active polymers is potentially useful for understanding and considering polymer morphology [24,25]. For example, Bu and coworkers [26] prepared three AIE-active conjugated poly(tetraphenylethene)s (*o*-PTPE, *m*-PTPE and *p*-PTPE) *via* Sonogashira cross-coupling polymerization with TPE as the monomer and different aryl diiodides as the linker, and the polymers can self-assemble to form nanospheres, hollow nanostructures and free-standing sheets by adjusting the solvent condition. Tang and coworkers [27] synthesized AIE-active polytriazole P(TPE–alanine) through a click reaction, which can be self-assembled into various architectures in THF/H_2O mixture like vesicles, "pear-necklace" and micro/nanofibers with the increase of water content. It is worth noting that most of the conjugated polymers with different morphologies

* Corresponding authors.
E-mail addresses: liuleijing@jlu.edu.cn (L. Liu), wjtian@jlu.edu.cn (W. Tian).

https://doi.org/10.1016/j.cclet.2020.09.019

were prepared through self-assembly by changing the solvent conditions or tuning the building blocks, but the weak constructive interactions often result in nanostructures that are not strong enough for practical applications [28]. Therefore, it is crucial to directly synthesize covalently bonded network polymers with different morphologies from small AIE-active monomers. Recently, Son and Ko [29] synthesized CMP tubes (CMP-AT) and bulk CMP-A powder with AIE properties by changing the synthetic procedures, and applied them for nitrotoluenes sensing. However, to our best knowledge, only few studies focused on developing AIE-active conjugated polymers with different morphologies by covalent crosslinking fluorescent molecules directly.

Given the above consideration, we prepared azine-linked conjugated organic network polymers with different morphologies based on AIE-active monomer TFBE and hydrazine linker, in the form of two-dimensional nanosheets, conjugated microporous polymers and conjugated organic frameworks. All of the three polymers with uniform architecture and unique AIE activity demonstrated high fluorescence quantum efficiency and favorable stability, and presented substantial selectivity and sensitivity toward nitro-explosive TNP.

Three conjugated polymers were prepared by Schiff base reaction based on the same AIE-active building block TFBE and hydrazine linker (Scheme 1) [31]. A simple method for the rapid synthesis of homogeneous nanosheets A-NS has been developed according to our previous works [15,30]. The scanning electron microscopy (SEM) micrographs of A-NS presented uniform and flattening sheet-like structures (Figs. 1a and b). Transmission electron microscopy (TEM) images of nanosheets also showed large-scale homogeneity and well-defined film morphology (Figs. 1c and d). It was also confirmed by atomic force microscopy (AFM) that the polymer nanosheets exhibited structural integrity and thinner slice architecture (Figs. 1e and f). The thickness of the layer polymer sheet obtained by AFM analysis was found to be about 5 nm.

Different from A-NS, A-CMP and A-COF are synthesized by solvothermal method under different solvent conditions. A-CMP was prepared in *o*-DCB/*n*-BuOH (4/1 by vol), while A-COF was synthesized in dioxane according to the previous literature [31]. A-CMP and A-COF presented uniformly distributed agglomerated nanometer-sized particles with overall morphology featured by SEM and TEM analysis (Fig. 2). TEM pictures at high magnification

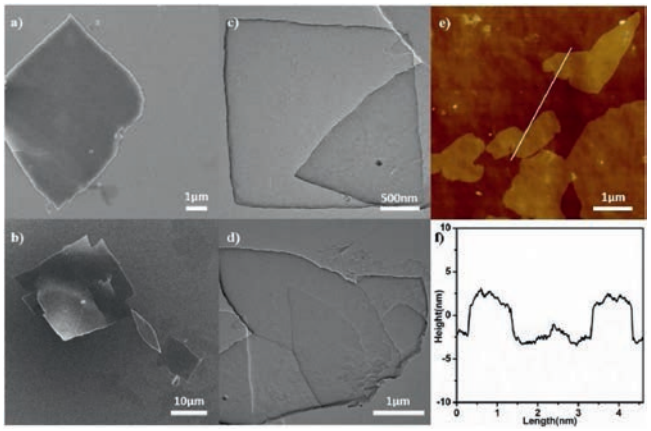

Fig. 1. (a,b) SEM image of A-NS at different scales. (c,d) TEM image of A-NS at different scales. (e) AFM image of A-NS. (f) Height profile along the line in the AFM image of polymer nanosheets.

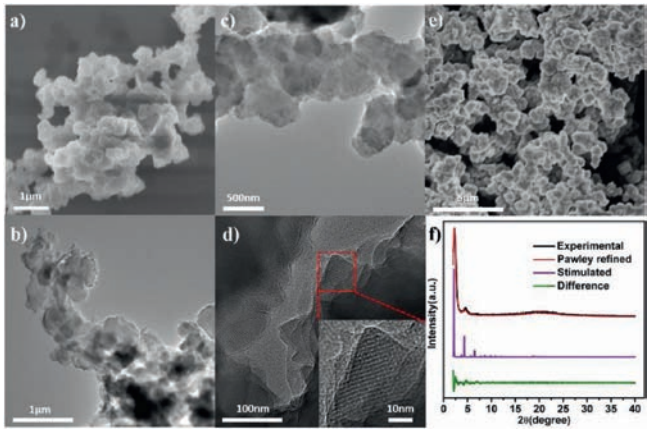

Fig. 2. (a) SEM and (b) TEM images of A-CMP. (c) TEM and (d) high-magnification TEM images of A-COF. (e) SEM image of A-COF. (f) The experimental pattern (black), Pawley refined pattern (red), simulated PXRD pattern for AA staggered structure (purple), and the difference plot between the experimental and refined patterns of A-COF (green).

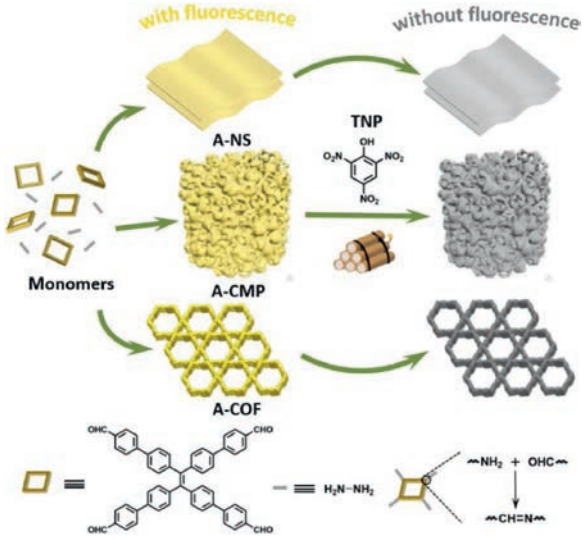

Scheme 1. Schematic representation with the structures of monomer and linker for the preparation of three fluorescent polymers and their application in the detection of TNP.

and PXRD data of A-COF revealed well-defined crystal lattice, indicating that A-COF possessed high crystallinity and uniformly ordered arrangement (Figs. 2d and f). A-COF exhibited strong XRD peaks at 2.3°, 4.6°, 6.9°, and 20.4°, which can be assigned to the (100), (200), (300) and (001) planes, respectively. The experimental PXRD profile matches well with the simulated data from the eclipsed AA stacking model, which is consistent with previous reported results (Fig. S3 in Supporting information) [31]. While, no diffraction peak can be seen on the PXRD patterns of A-CMP and A-NS, demonstrating that they are amorphous (Fig. S4 in Supporting information).

As shown in Fig. S5 (Supporting information), the successful synthesis of the polymers under different conditions was demonstrated by Fourier transform infrared spectroscopy (FTIR). The characteristic C=N stretching vibrations of the azine group at around 1620 cm^{-1} indicated that azine linkages are definitely formed in the three conjugated polymers. The UV–vis absorption and PL spectra of A-NS, A-CMP and A-COF showed a gradually red shift owing to the increased π-π interactions between the benzene rings (Figs. S6 and S7 in Supporting information) [17]. The fluorescence quantum yields of A-NS, A-CMP, and A-COF were measured to be 6.31%, 5.26%, and 5.80%, respectively (Table S1 in Supporting information). The porosity of A-CMP and A-COF were

carried out by nitrogen sorption measurements at 77 K. As shown in Fig. S8 (Supporting information), the BET surface area was estimated to be 137.29 m^2/g for A-NS, 109.44 m^2/g for A-CMP and 599.87 m^2/g for A-COF, respectively. Thermal gravimetric analysis (TGA) profile showed that the three polymers showed no obvious weight loss before 200 °C, suggesting the polymers exhibited good thermal stability (Fig. S9 in Supporting information).

It is known that azine-linked molecules can be deserved as chemo-sensing detector due to their open nitrogen atoms in azine moieties [32,33]. As can be seen in Figs. S10–S12 (Supporting information), EDS mapping images of the three polymers revealed that N was homogeneously dispersed within the polymers. Taking advantage of their high fluorescence and generous contact sites, azine-linked conjugated polymers were exploited as fluorescence sensors for explosive detection. To examine detection capabilities of the three polymers, TNP with hydroxy units was chosen as the model explosive compound. The fluorescence quenching behaviors of the three polymers for TNP were investigated in ethanol solution because of good stability and dispersion of polymers in ethanol. The PL intensities of the three polymers progressively decreased with TNP being added gradually (Fig. 3 and Fig. S13 in Supporting information). And A-NS showed the best fluorescence quenching response to TNP (Fig. 3a). The fluorescence of A-NS was almost wholly quenched when the TNP concentration reaches only 22 μmol/L. The Stern-Volmer plot (K_{sv}) of A-NS exhibited a linear correlation with a quenching constant of 8×10^5 L/mol at low concentrations of TNP (Fig. 3b). The limit of detection (LOD) value of A-NS for TNP has been determined to be 0.09 μmol/L. K_{sv} of A-CMP and A-COF acquired from the Stern-Volmer plots was calculated as 4.7×10^5 L/mol and 5.4×10^5 L/mol, respectively. And the detection limits were found to be 0.19 μmol/L for A-CMP and 0.17 μmol/L for A-COF. A-NS with thin-sheet like morphology has more contact opportunity with TNP and the dangling azine groups on the surface of two-dimensional polymer nanosheets can strongly interact with TNP, while TNP is difficult to diffuse into the bulk porous material such as A-CMP and A-COF although they have inner micro porosity [29,34]. Thus, A-NS showed more rapid and sensitive fluorescence quenching response to TNP compared with A-CMP and A-COF.

To explore the selectivity of the azine-linked conjugated polymers, further fluorescence behavior was examined in the presence of various nitroaromatic compound 4-nitrotoluene (NT), 2,4-dinitrotoluene (DNT), *p*-nitrobenzaldehyde (FNB), *m*-dinitrobezene (DNB), 4-chloronitrobenzene (NCB), 2,4-dinitrochlorobenzene (DNCB), 4-nitrophenol (NP), and 2,4-dinitrophenol (DNP), and their molecular structure were presented in Fig. S14 (Supporting information). The fluorescence intensity of three polymers was changed obviously after being added TNP, while the other nitroaromatic compounds exhibited slight effect to the fluorescence intensity of the polymers (Fig. 4). The sensing performance of the three azine-linked polymers as well as other conjugated

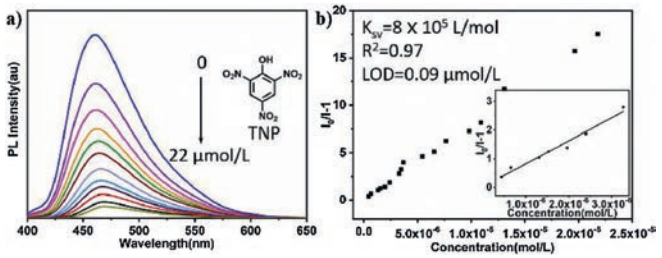

Fig. 3. (a) Fluorescence spectra of A-NS in ethanol phase (c =0.04 mg/mL) as the adding of TNP. (b) The Stern-Volmer plots of (I_0/I-1) values *versus* TNP concentrations (inset: the enlarged Stern-Volmer plots *versus* low TNP concentrations).

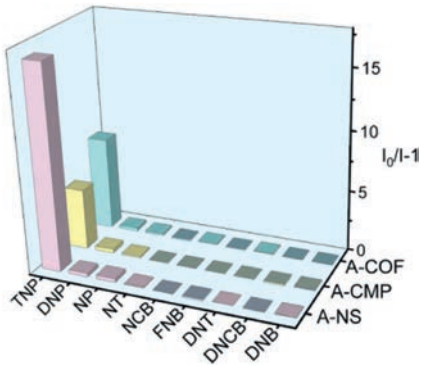

Fig. 4. Fluorescence intensity changes of three polymers induced by different nitroaromatic compounds. The concentration of nitroaromatic analytes is 22 μmol/L.

polymers with different morphologies for TNP were listed in Table S2 (Supporting information), and the polymers in present work exhibited higher K_{sv} compared with other polymer-based sensors, demonstrating that azine-linked polymers are highly selective and sensitive sensors for TNP detection.

To shed insights on the fluorescence quenching mechanism, we intercepted the model compound whose molecular structure was contained in the three polymers and studied the interaction between TNP and the model compound by MOE. Fig. 5 and Fig. S15 (Supporting information) showed 2D and 3D styles of model compound/TNP complex with the lowest energy. It can be found that the intermolecular forces between TNP and model compound are mostly made up of hydrogen-bonding between hydroxyl of TNP and the azine moieties of model compound. Compared with other nitroaromatic analytes, TNP exhibited more strong interactions with azine edges because of the electron deficient nature of TNP came from three substituted -NO_2 groups with strong electron-withdrawing tendency, indicating that TNP is easily combined with polymer to form ground-state complex which facilitates the fluorescence quenching [32,35]. The fluorescence lifetimes of the three polymers illustrated the quenching dynamics (Table S3 and Fig. S16 in Supporting information). The lifetimes of the three polymers remain almost unchanged with the presence and absence of TNP, which is consistent with the ground-state complexation in the static fluorescence quenching. The combination of TNP with the azine-linked polymers forms non-emissive complex that traps the excitation energy of the skeletons of the polymeric network, resulting in the fluorescence quenching process [32,36,37].

In summary, we synthesized three azine-linked conjugated network polymers with distinct morphologies by using the same building block AIE-active TFBE and hydrazine through changing the synthetic condition. The three polymers displayed high fluorescence quenching selectivity and sensitivity toward TNP due to the hydrogen-bonding interactions between polymers and

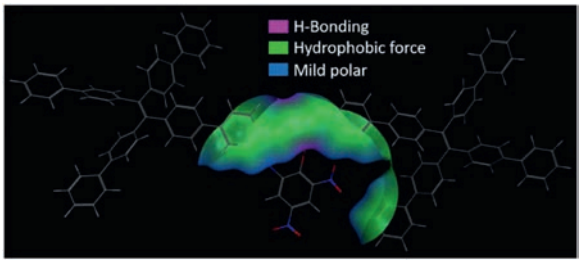

Fig. 5. Three-dimensional image showing the interactions between the model compound and TNP.

TNP. The best TNP sensing performance with the Stern-Volmer constants (K_{sv}) values up to 8×10^5 L/mol and a detection limit of 0.09 μmol/L was obtained for A-NS. It is unique to construct polymer systems with different morphologies based on the same monomer by covalent crosslinking polymerization, and we believe that developing AIE-active conjugated polymers with various morphologies will be worthy of expectation.

Declaration of competing interest

The authors report no declarations of interest.

Acknowledgments

This work was financially supported by the National Natural Science Foundation of China (Nos. 21835001, 51773080, 21674041), Program for Changbaishan Scholars of Jilin Province, and by the "Talents Cultivation Program" of Jilin University.

Appendix A. Supplementary data

Supplementary material related to this article can be found, in the online version, at doi:https://doi.org/10.1016/j.cclet.2020.09.019.

References

[1] C. Wang, H. Dong, W. Hu, Y. Liu, D. Zhu, Chem. Rev. 112 (2012) 2208–2267.
[2] L. Li, Z. Cai, Q. Wu, et al., J. Am. Chem. Soc. 138 (2016) 7681–7686.
[3] V. Kumar, B. Maiti, M.K. Chini, P. De, S. Satapathi, Sci. Rep. 9 (2019) 7269.
[4] C. Zhang, Y. He, P. Mu, et al., Adv. Funct. Mater. 28 (2018) 1705432.
[5] D. Ding, K. Li, W. Qin, et al., Adv. Healthc. Mater. 2 (2013) 500–507.
[6] Y.F. Xie, S.Y. Ding, J.M. Liu, W. Wang, Q.Y. Zheng, J. Mater. Chem. C 3 (2015) 10066–10069.
[7] X. Guan, H. Li, Y. Ma, et al., Nat. Chem. 11 (2019) 587–594.
[8] G. Chen, H.H. Lan, S.L. Cai, et al., ACS Appl. Mater. Interfaces 11 (2019) 12830–12837.
[9] X. Liu, Y. Xu, D. Jiang, J. Am. Chem. Soc. 134 (2012) 8738–8741.
[10] M. Faheem, S. Aziz, X. Jing, et al., J. Mater. Chem. A 7 (2019) 27148–27155.
[11] D.T. McQuade, A.E. Pullen, T.M. Swager, Chem. Rev. 100 (2000) 2537–2574.
[12] R. Hu, A. Qin, B.Z. Tang, Prog. Polym. Sci. 100 (2020) 101176.
[13] K. Baek, I. Hwang, I. Roy, D. Shetty, K. Kim, Acc. Chem. Res. 48 (2015) 2221–2229.
[14] T. Chen, H. Yin, Z.Q. Chen, et al., Small 12 (2016) 6547–6552.
[15] S. Jiang, S. Liu, L. Meng, et al., Sci. China Chem. 63 (2020) 497–503.
[16] M. Wang, H.T. Zhang, L. Guo, D.P. Cao, Sens. Actuators B: Chem. 274 (2018) 102–109.
[17] J. Dong, K. Zhang, X. Li, et al., Nat. Commun. 8 (2017) 1142.
[18] T.M. Geng, S.N. Ye, Y. Wang, et al., Talanta 165 (2017) 282–288.
[19] C. Liang, H. Lin, Q. Wang, et al., J. Hazard. Mater. 381 (2020) 120983.
[20] S. Fu, Y. Zhang, S. Guan, et al., ACS Appl. Mater. Interfaces 10 (2018) 14281–14286.
[21] K.C. Huang, C.W. Hu, C.Y. Tseng, et al., J. Mater. Chem. 22 (2012) 14727–14733.
[22] K. Dey, H.S. Kunjattu, A.M. Chahande, R. Banerjee, Angew. Chem. Int. Ed. 59 (2020) 1161–1165.
[23] S. Kandambeth, V. Venkatesh, D.B. Shinde, et al., Nat. Commun. 6 (2015) 6786.
[24] J. Li, J. Wang, H. Li, et al., Chem. Soc. Rev. 49 (2020) 1144–1172.
[25] H.T. Feng, J.W.Y. Lam, B.Z. Tang, Coord. Chem. Rev. 406 (2020) 213142.
[26] X. Liu, L. He, C. Wang, et al., J. Mater. Chem. C 5 (2017) 3156–3166.
[27] Q. Liu, Q. Xia, S. Wang, B.S. Li, B.Z. Tang, J. Mater. Chem. C 6 (2018) 4807–4816.
[28] S.J. Rowan, S.J. Cantrill, G.R.L. Cousins, J.K.M. Sanders, J.F. Stoddart, Angew. Chem. Int. Ed. 41 (2002) 898–952.
[29] S.H. Ryu, D.H. Lee, Y.J. Ko, et al., Macromol. Chem. Phys. 220 (2019) 1900157.
[30] S. Liu, S. Jiang, J. Xu, et al., Macromol. Rapid Commun. 40 (2019) 1800892.
[31] J.Q. Dong, X. Li, S.B. Peh, et al., Chem. Mater. 31 (2019) 146–160.
[32] S. Dalapati, S.B. Jin, J. Gao, et al., J. Am. Chem. Soc. 135 (2013) 17310–17313.
[33] B. Gole, S. Shanmugaraju, A.K. Bar, P.S. Mukherjee, Chem. Commun. 47 (2011) 10046–10048.
[34] C. Anichini, W. Czepa, D. Pakulski, et al., Chem. Soc. Rev. 47 (2018) 4860–4908.
[35] S. Shanmugaraju, C. Dabadie, K. Byrne, et al., Chem. Sci. 8 (2017) 1535–1546.
[36] H. Sohn, M.J. Sailor, D. Magde, W.C. Trogler, J. Am. Chem. Soc. 125 (2003) 3821–3830.
[37] B. Valeur, Molecular Fluorescence: Principles and Applications, Wiley, Weinheim, 2005.